PCCP

Accepted Manuscript

ROYAL SOCIETY OF CHEMISTRY

www.rsc.org/pccp

PCCP

ARTICLE

Non-thermal Ion Desorption From an Acetonitrile (CH_3CN) Astrophysical Ice Analogue Studied by Electron Stimulated Ion Desorption

Received 00th January 20xx,
Accepted 00th January 20xx

DOI: 10.1039/x0xx00000x

www.rsc.org/

F. de A. Ribeiro,[a,b] G. C. Almeida,[a,c] Y. Garcia-Basabe,[a,d] W. Wolff,[e] H. M. Boechat-Roberty[f] and M. L. M. Rocco[a]*

The incidence of high-energy radiation onto icy surfaces constitutes an important route for leading new neutral or ionized molecular species back to the gas phase in interstellar and circumstellar environments, especially where thermal desorption is negligible. In order to simulate such processes, an acetonitrile ice (CH_3CN) frozen at 120 K is bombarded by high energy electrons, and the desorbing positive ions are analyzed by time-of-flight mass spectrometry (TOF-MS). Several fragment and cluster ions were identified, including the $H_{n\,=\,1\text{-}3}^+$, $CH_{n=0\text{-}3}^+/NH_{n=0\text{-}1}^+$; $C_2H_{n=0\text{-}3}^+/CH_{n=0\text{-}3}N^+$, $C_2H_{n=0\text{-}6}N^+$ ion series and the ion clusters $(CH_3CN)_{n=1\text{-}2}^+$and $(CH_3CN)_{n=1\text{-}2}H^+$. The energy dependence on the positive ion desorption yield indicates that ion desorption is initiated by Coulomb explosion following Auger electronic decay. The results presented here suggest that non-thermal desorption processes, such as desorption induced by electronic transitions (DIET) may be responsible for delivering neutral and ionic fragments from simple nitrile-bearing ices to the gas-phase, contributing to the production of more complex molecules. The derived desorption yields per electron impact may contribute to chemical evolution models in different cold astrophysical objects, especially where the abundance of CH_3CN is expected to be high.

Introduction

Acetonitrile (CH_3CN), also known as methyl cyanide, is the simplest organic molecule bearing the nitrile (–C≡N) functional group. Due to its high dipole moment (3.91 Debye), the rotational transition emission lines (in the millimetre and sub-millimetre wavelength range) of CH_3CN are a good probe for estimating gas temperature and density towards molecular clouds in the interstellar-medium (ISM),[1] turning CH_3CN into a relevant astrophysical molecule.

The first detection of millimetre emission lines of CH_3CN was made by Solomon et al.[2] towards Sgr A and Sgr B molecular clouds. Since that time, CH_3CN has also being detected towards a number of sources, including cold starless molecular clouds,[3] high[1, 4, 5] and low-mass[6, 7] proto-stars and extragalactic sources.[8] Acetonitrile is also a prominent molecule in the Titan's atmosphere,[9] and in the coma of Kohoutek[10] and Hale-Bopp[11] comets. Recently, CH_3CN has also been identified in the *in situ* analysis of the 67P/Churyumov-Gerasimenko comet by the COSAC experiment onboard the Philae lander.[12] The latter is particularly interesting, since recent observations of CH_3CN and HCN toward the boundaries of the protoplanetary disk around the young star MWC 480 showed similar abundance ratios in comparison to Solar System comets.[13] This fact points to a connection between the interstellar and planetary material, and leaves an open question regarding how complex molecules may survive and evolve from the early stages of star formation up to their presence in planetary systems.

Inside dense molecular clouds, most molecules are expected to directly freeze out onto the surface of cold dust grains,[14] forming ice mantles. Nonetheless, there is also the possibility of *in situ* formation of CH_3CN by the radiative association reaction $CH_3 + CN \rightarrow CH_3CN$, and by hydrogenation of C_2N on grains at earlier times of star-formation.[15] Though any CH_3CN infrared absorption band has been detected up to date, the cyanate anion OCN^- is commonly detected in ices towards a number of sources,[16] indicating that a nitrile chemistry network might be occurring in the ISM. Both interstellar and planetary ice mantles are exposed to several ionizing agents, such as ultraviolet (UV) radiation, stellar winds, cosmic ray bombardment and charged particles magnetically trapped in planetary magnetospheres.[17] All these radiation sources deposit energy into ices, leading to a more complex chemistry.

Several attempts have been made in order to understand the energetic and dynamics of the fragmentation of CH_3CN by

[a] Instituto de Química, Universidade Federal do Rio de Janeiro, 21941-909 Rio de Janeiro, RJ Brazil. E-mail: luiza@iq.ufrj.br
[b] Instituto Federal de Educação, Ciência e Tecnologia do Rio de Janeiro, 20270-021, Rio de Janeiro, RJ - Brazil.
[c] Departamento de Física, Pontifícia Universidade Católica, 22451-900, Rio de Janeiro, RJ Brazil.
[d] Instituto Latino-Americano de Ciências da Vida e da Natureza, Universidade Federal da Integração Latino-Americana, 85867.970, Foz do Iguaçu, PR – Brazil
[e] Instituto de Física, Universidade Federal do Rio de Janeiro, 21941-909 Rio de Janeiro, RJ Brazil.
[f] Observatorio do Valongo, Universidade Federal do Rio de Janeiro, 20080-090 Rio de Janeiro RJ Brazil
† Electronic Supplementary Information (ESI) available. See
DOI: 10.1039/x0xx00000x

ionizing radiation.[18-23] On the condensed medium, a few studies have focused on the correlation between ion desorption and Auger electron emission after localized electronic excitation employing synchrotron radiation.[24-26] Previous laboratory studies were also dedicated in understanding the energetic processing of CH_3CN ices under conditions that mimic those found in astrophysical environments. Hudson et al.[27] noted CH_3NC isomerisation and the production of $H_2C{=}C{=}NH$ (ketenimine), CH_4 and HCN products in the CH_3CN ice bulk by both UV photolysis and 0.8 MeV proton bombardment. Similar results were achieved by Abdugalil et al.[28] employing the reflection–absorption infrared spectroscopy (RAIRS) technique before and after 200 keV proton irradiation of frozen CH_3CN deposited at 15 K. On the other hand, Abdugalil et al.[28] noted that the electron irradiation in the 250-400 eV energy range leads only to CH_3CN surface removal by electron-promoted desorption. Since the RAIRS technique probes only the remaining ice material after electron irradiation, the authors could not conclude about the nature of the desorbing species.

Electrons impinging on a surface transfer part of their energy and momentum to the target by inelastic scattering collisions that may result in molecular ionization. In case of core level ionizations, such high energy states may decay through Auger electron emission, whose final state is characterised by localized multiple valence holes. The mutual electrostatic repulsion between unscreened valence holes is the basis for Coulomb explosion, leading to molecular bond breakage and desorption of neutral and ionic species.[29] This ion desorption mechanism is generally known as the Auger Stimulated Ion Desorption (ASID) mechanism. Non-thermal desorption processes, such as desorption induced by electronic transitions (DIET), is thought to play a role in delivering surface processed material back to the gas-phase of dense regions in the ISM.[30] For instance, ion emission from regolith analogs of the Mercury surface by fast electron impact has been claimed[31] as a possible mechanism contributing to the formation of the planet exosphere.

In this work we investigate the fragment and cluster ion desorption from the surface of a CH_3CN ice by means of the Electron Stimulated Ion Desorption (ESID) technique. The CH_3CN ice film was grown *in situ* at 120 K, which is close to the thermal desorption peak of CH_3CN at approximately 135 K under laboratory conditions[28]. In these circumstances, similar non-thermal desorption processes, as studied here by ESID, are expected to occur during the warm-up phase of the inner envelope of pre-stellar cores prior to the hot core phase, when ice mantles are up to sublimate. Implications for Titan's chemistry are also highlighted.

Experimental

In this study, an acetonitrile (CH_3CN) ice analogue is bombarded by a pulsed electron beam, and the positive ions desorbed from the icy surface are analyzed by time-of-flight mass spectrometry (TOF-MS). The experimental setup consists of an XYZ sample manipulator connected to a liquid nitrogen cooling system, a commercial electron gun (Kimball Physics, ELG-2), and a linear time-of-flight mass spectrometer. All instruments are housed in an ultrahigh vacuum (UHV) chamber at 1.0×10^{-9} mbar base pressure.

The liquid CH_3CN sample was purchased from Sigma-Aldrich with purity greater than 99.8%, which was further degassed through several freeze–pump–thaw cycles before admission into the UHV chamber with a leak valve. The vapour entrance is monitored by a residual gas analyzer (RGA) and the ice analogue is grown by directly condensation of background CH_3CN molecules onto the 120 K cooled metallic substrate of the sample manipulator. Once the pressure inside the chamber was kept at ~ 5 x 10^{-8} mbar during 5 minutes of sample dosing, this exposure leads accordingly to an ice thickness of 11 Langmuir (1 Langmuir = 10^{-6} Torr·s), assuming a sticking coefficient equal to unity for CH_3CN at 120 K.

The time-of-flight mass spectrometer consists of an electrostatic extraction system, a collimating lens pair, a drift tube of 25 cm length, and two microchannel plate detectors (MCPs) disposed in the chevron configuration. Positively charged desorbing ions are extracted by a constant positive electrical potential (+1900 V) applied to the sample. After extraction, the positive ion beam traverses three metallic grids (each one with 90% nominal transmission) before reaching the MCP detector. The grid entrance of the TOF tube (grounded) is sited 10 mm away from the sample surface, and the major axis of the TOF tube is parallel to the surface normal. The positive potential applied on the sample also accelerates the incident electron beam, enhancing the final impact energy.

The incident electron beam impinges onto the sample surface focused in a 0.5 mm spot size and with an angle of 60° with respect to the surface normal. We used the CASINO code[32] to simulate the electron trajectories within the ice under the experimental conditions described previously. The results give a distribution maximum at a penetration depth of 80 nm for 2300 eV electrons in a CH_3CN ice of 0.8 g cm^{-3} density.[27]

An external pulse generator (Hewlett-Packard, HP 8116A) is responsible for triggering and pulsing the electron beam with a 20 ns pulse width within a time repetition rate of 80 kHz (12.5 µs). Thus, the pulse generator is also responsible for supplying the start signal of the time-to-digital converter device (TDC), with a 12.5 µs time window for ions arrival. Each ion generates an output detector signal, which is processed by standard pulse counting electronics and used as the stop signal of the TDC device. More details about the available experimental setup can be found elsewhere.[33]

The positive ion desorption yield Y_i (ions/electron) for each desorbed ion was derived directly from the time-of-flight (TOF) mass spectrum by the standard expression[33, 34]:

$$Y_i = \frac{A_i}{n_{starts} n_{e^-}} \quad (1)$$

where A_i is the integrated peak area for each desorbed ion i in the TOF mass spectrum; n_{starts} is the number of start signals of

the TDC device and n_{e^-} is the number of incident electrons in the electron beam at each start signal, derived by measuring the incident electron beam current. A typical electron beam current of 9.6 nA result in 7.5 x 10^5 incident electrons. Ions assignment and their respective Y_i values at 2300 eV electron impact energy are listed in Table S1 (available on the electronic supplementary information).

Results and discussion

The electron-stimulated ion desorption (ESID) spectrum of positive ions from the CH_3CN ice is presented in Figure 1. It can be divided into four groups, in which each group corresponds to the fragmentation of the CH_3CN molecule into different ion series. The first group is the $H_{n\ =\ 1\text{-}3}^+$ ion series and the remaining are ascribed to the $CH_{n=0\text{-}3}^+/NH_{n=0\text{-}1}^+$; $C_2H_{n=0\text{-}3}^+/CH_{n=0\text{-}3}N^+$ and the $C_2H_{n=0\text{-}6}N^+$ ion series. Some of the ions within each ion series have already been observed during the gas phase fragmentation of the CH_3CN with soft X-rays,[21, 23] ultraviolet radiation[19] and by electron impact[20] and, thus, it is assumed that these ions originate from the direct fragmentation of isolated CH_3CN molecules.

A minor amount of water from the residual gas of the UHV chamber also co-deposit with CH_3CN during the ice growth. Water contribution is noted by the presence of the fragments m/z = 16, 17, 18 and 19, attributed to O^+, OH^+, H_2O^+ and H_3O^+, respectively. On the other hand, the present relative ratios Y_{O+}/Y_{H3O+}, Y_{OH+}/Y_{H3O+} and Y_{H2O+}/Y_{H3O+} are clearly different for the ESID of pure water ice.[35-39] Moreover, the other members of the water cluster ion series $(H_2O)_n^+$ and $(H_2O)_nH^+$ with n ≥ 2 are absent,[40, 41] probably because water molecules are well diluted on the frozen CH_3CN surface. In this framework, Mejías et al.[42] showed that a single proton tends to stay bonded to H_2O to form H_3O^+ when solvated by more than one CH_3CN molecule. This trend is thought to increase the H_3O^+ desorption probability in the present case.

The most intense desorbed fragment is the H^+ ion, what is consistent with the formation of a thick molecular film.[43] Also, light fragments, such as H^+ and H_2^+, have high initial kinetic energy, what lowers their residence time on surface, lessening their probability of neutralization.[44] In addition to H^+ and H_2^+, the H_3^+ ion was also produced as a member of the $H_{n\ =\ 1\text{-}3}^+$ ion series.

It is noteworthy that the present H_3^+ ion desorption yield from CH_3CN is almost the same for CH_3OH ice, as measured by Almeida and co-workers.[34] Eland et al.[45] proposed that the H_3^+ ion comes from charge separation of doubly charged precursor ions, mainly when the partner ion formed with H_3^+ is thermodynamically stable. Pilling et al.[46] have also observed the production of H_3^+ by the dissociation of core-excited organic molecules containing the methyl group, including CH_3CN. These observations correlates well with a general desorption mechanism, in which H_3^+ originates from the dissociation of the methyl group during the fragmentation of the multiply charged parent molecule.

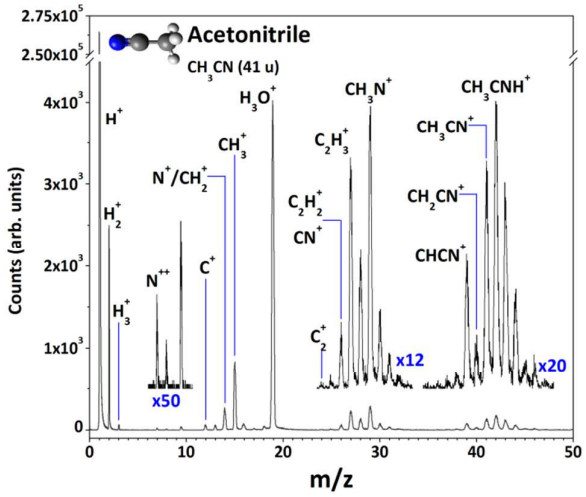

Figure 1. Electron Stimulated Ion Desorption (ESID) spectrum up to m/z = 50 of frozen CH_3CN at 120 K by 2300 eV electron impact energy. Some regions of the spectrum have been expanded in the sake of clarity and their scaling factors are shown in blue. The assignment of the desorbed ions is given in Table S1.

In case of normal Auger electronic decay of the core ionized CH_3CN molecule, this process may lead to a final state with two localized valence holes (2h) in a bonding orbital, whose unscreened hole-hole repulsion results in charge separation and ion desorption by Coulomb explosion. The doubly charged parent molecule (CH_3CN^{++}) has not been identified, though its formation may not be ruled out, due to the presence of the doubly charged N^{++} fragment (see Figure 1).

The positive ion yield as a function of the electron impact energy in the energy range from 1000 to 1800 eV is presented in Figure 2. Each curve in Figure 2 represents the sum over all desorbed fragments in each ion series (CH_n^+, $C_2H_n^+/H_nCN^+$ and $C_2H_nN^+$, respectively).

As can be noted in Figure 2, there is a desorption increase for all ion series at 1400 eV, which is 3.5 times the ionization threshold for the CH_3CN N1s core level at 406 eV.[21] Typically, the electron impact ionization cross-section reaches a broad maximum at energies 3 – 4 times the energy required for photoionization.[47] Therefore, all fragmentation channels are enhanced at 1400 eV electron impact energy, especially those channels involving the rupture of the C≡N bond, resulting in $C_2H_n^+$ desorption. As the electron impact energy is increased up to 1800 eV, there is a drop in the positive ion desorption yield for $C_2H_nN^+$ and CH_n^+ ion series, while the $C_2H_n^+/H_nCN^+$ positive ion yield remains almost the same within the experimental error. The latter is probably due to ionizations caused by secondary electrons produced in the CH_3CN ice bulk. Secondary electrons lead mainly to valence-shell ionizations[48] and, thus, only soft fragmentation is expected. As a result, there is a minor production of the atomic fragments from the CH_n^+ ion series, and the excited parent molecule will dissociate preferentially in the $C_2H_n^+/H_nCN^+$ ion series.

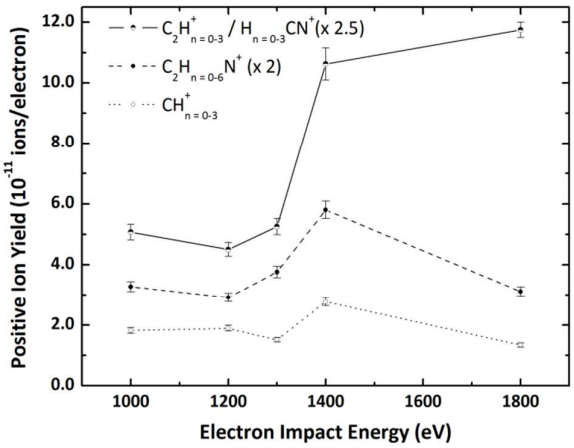

Figure 2. Positive ion desorption yield curves as a function of the incident electron impact energy in the range 1000-1800 eV. Each curve presents the summation of the desorption yield of all ions comprised within each ion series (CH_n^+, $C_2H_n^+/H_nCN^+$ and $C_2H_nN^+$). See text for more details.

The first group in the ESID spectrum of Figure 1 is composed by intense and light fragment ions, showing strong fragmentation of the CH_3CN molecule on surface. The range from m/z = 12 to m/z = 15 is attributed to the CH_n^+ ion series (n = 0-3), which is caused by C–C bond cleavage and hydrogen elimination. The most intense ion of the CH_n^+ ion series is CH_3^+, followed by CH_2^+, C^+ and CH^+, respectively. This behaviour is quite different from the one observed by Almeida and co-workers[34] for ion desorption from CH_3OH ice, in which the intensity sequence follows CH_3^+, CH_2^+ CH^+ and C^+. The presence of an additional carbon in the C≡N group of CH_3CN increases the C^+ desorption for CH_3CN in respect to CH_3OH. Moreover, assuming that a similar mechanism rules the ion dissociation of the methyl group of CH_3CN and CH_3OH, and that the ions from the CH_n^+ ion series in both cases have the same desorption probability, one finds that the ratio Y_{13}/Y_{15} for CH_3OH is greater than the same ratio for CH_3CN (0,22 and 0,064, respectively). This m/z range for CH_3CN may also contain the ions N^+ and NH^+ at m/z = 14 and m/z = 15, resulting from C≡N bond cleavage and proton transfer to CH_3CN, respectively.

A very pronounced intensity alternation between odd and even-mass fragment ions is observed in the range from m/z = 24 to 29. Such pattern is generally observed for the desorption of ions from the $C_2H_n^+$ ion series, in which odd-mass fragments are more abundant than even-mass fragments[49] due to the production of more stable closed-shell ions with odd number of hydrogen atoms[50], which yield odd-numbered m/z ions. On the other hand, the stoichiometry of the CH_3CN molecule itself cannot lead directly to $C_2H_n^+$ ions with n ≥ 4, and N-bearing fragments might also be present. Indeed, Rider et al.[19] and Kukk et al.[26] attributed the ion peak at m/z = 28 to the CH_2N^+ ion during the gas phase photofragmentation of CH_3CN. This is an interesting feature, since the production of ions from the CH_nN^+ ion series require hydrogen migration during fragmentation and desorption. Therefore, the m/z range from 24 to 27 is attributed to the $C_2H_n^+$ (n = 0 – 3) ion series along with the CH_nN^+ (n = 0 – 4) ion series.

The last ion series presented in Figure 1 is attributed to the parent ion region CH_nCN^+, in which the ions of m/z ratio up to 40 originate from the sequential loss of hydrogen atoms by the parent ion CH_3CN^+ (m/z = 41). Another possibility for the m/z = 41 ion peak would be desorption of CH_3NC^+. The isomerization of CH_3CN into CH_3NC under 200 keV proton and UV irradiation was already reported in the literature by Hudson and Moore[27] and Abdulgalil et al.[28] But, it is noteworthy that whichever any CH_3CN^+ or CH_3NC^+ (m/z = 41) is desorbing, with only Time-of-Flight mass spectrometry it is not possible to distinguish them.

As can be seen in Figure 1, the same even-odd intensity alternation is not observed anymore, as the most intense ion within this series appears at m/z = 42. Interestingly, since nitrogen has an odd-number of valence electrons, N-bearing positive fragments are more stable at even m/z values, and the parent molecule tends to desorb in the protonated form, CH_3CNH^+.

The greater ion desorption yield of CH_3CNH^+ in respect to CH_3CN^+ also suggests that neighbouring CH_3CN molecules might be strongly bound by C–H···N intermolecular forces on the ice surface. This fact contribute to the proton-transfer reaction – $CH_3CN^+ + CH_3CN \rightarrow CH_3CNH^+ + CH_2CN$ – between an ionized acetonitrile molecule and its neutral neighbour, leading to a more stable ion with a proton bounded to the neutral parent molecule. The production of protonated acetonitrile as the result of ion-molecule reactions in the gas-phase was reported by Ascenzi and co-workers[51], in which they observed the same threshold appearance energy for both CH_3CN^+ and CH_3CNH^+ at about 12.2 eV photon energy. Such reactions are certainly favoured in the condensed medium, since the intermolecular distance among CH_3CN molecules might be considerably reduced and there is an excess of protons being formed and solvated by CH_3CN. The strong ion-dipole interaction between H^+ and CH_3CN comes from the strong proton affinity of CH_3CN. Thus, the proton transfer and the ion desorption might occur through a similar mechanism to what has been proposed for H_3O^+ desorption from H_2O ice.[52] Coulomb repulsion between such solvated protons occurs on the surface during or after the separation of valence holes created by Auger decay.

The electron-stimulated desorption of fragments from a surface is an isolated event, governed by single electron-impact events.[37, 38, 53] Therefore, an increase in the flux of impinging electrons should be correlated with a linear enhance of the amount of desorbed ions. The relative ion desorption yield N_i (ions/start) for C_2N^+, $CHCN^+$, CH_2CN^+, CH_3CN^+ and CH_3CNH^+ as a function of the electron beam current I (nA) impinging on the ice surface at 2300 eV electron impact energy is shown in Figure 3. The integrated area for each ion peak was normalized by the number of start signals of the TDC device and, thus, it represents the average amount of ions desorbed within a time-of-flight window.

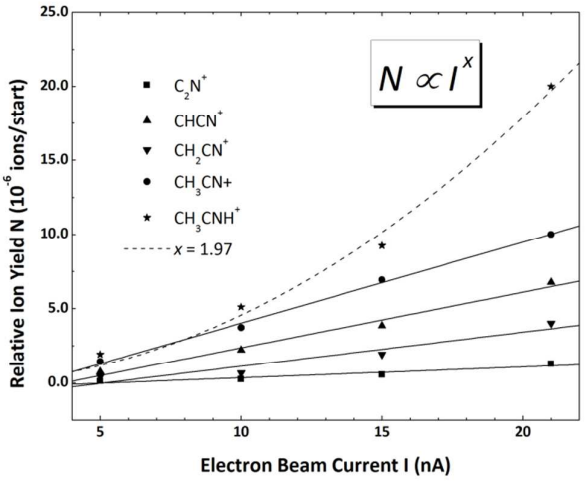

Figure 3. Relative ion desorption yield N_i for the ions comprised in the parent ion region (CH_nCN^+) as a function of the incident electron beam current at 2300 eV electron impact energy.

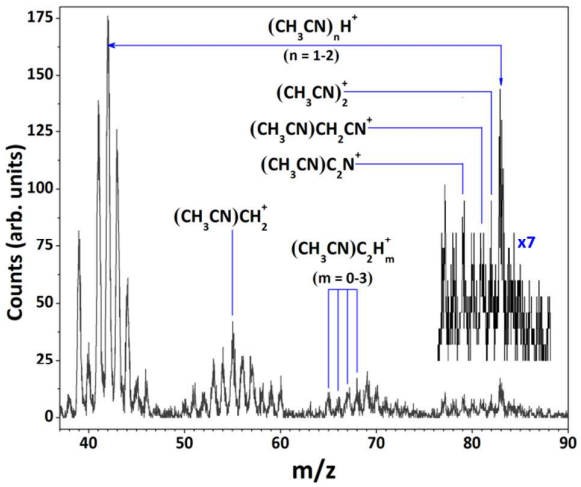

Figure 4. ESID spectrum of frozen CH_3CN at 120 K by 2300 eV electron impact energy showing desorbed ions from m/z = 37 up to m/z = 90. The last region of the spectrum was expandend by a factor of seven in order to highlight the desorption of $(CH_3CN)_2^+$ and $(CH_3CN)_2H^+$ dimer cations. The assignment of the desorbed ions is given in Table S1.

As already expected, the greater the electron beam current (which is directly proportional to the flux of incident electrons), more ions desorb from the ice surface at each start signal. A linear dependence on the electron beam current is seen for all desorbed ions of the CH_nCN^+ (n = 0-3) ion series, suggesting that these ions result from the direct CH_3CN molecular fragmentation on surface. On the other hand, the CH_3CNH^+ relative ion desorption yield seems to obey a power law in respect to the incident electron beam current, $N_i \propto I^x$, in which x is the power law exponent.

As indicated in Figure 3, the relative ion yield dependence of CH_3CNH^+ on the electron beam current exhibits almost a quadratic growth. Such nonlinear dependence has already been observed for low energy electron-stimulated anion desorption,[54] fs-laser induced associative desorption[55] and ion desorption following ultra-short XUV laser pulses,[56, 57] indicating that collisions and/or reactions between more than one dissociating products may lead to a more complex desorption framework. In this sense, this scenario may be consistent with the framework of proton-transfer reactions between dissociating species during ion desorption as the first step towards the production of more complex species, such as cluster ions.

The ESID spectrum of CH_3CN acquired at the same conditions of Figure 1, but now extended from m/z = 37 to m/z = 90 is presented in Figure 4. The high-energy electron bombardment of frozen CH_3CN stimulates the ion desorption of cluster ions. The presence of the latter is attributed to the interaction between outgoing fast desorbed ions and neutral CH_3CN molecules on the top ice surface. The region between 50 ≤ m/z ≤ 60 corresponds to the association of a neutral CH_3CN molecule to ions from the CH_n^+/NH_n^+ ion series, while the ions appearing at 65 ≤ m/z ≤ 72 correspond to the association of the neutral CH_3CN to ions from the $C_2H_n^+/CH_nN^+$ ion series.

A set of suggested reaction routes to more complex nitriles starting from CH_3CN is shown in the scheme 1. For instance, the high intensity ion peaks at m/z = 54 and 55, assigned to the cluster ions $(CH_3CN)CH^+$ and $(CH_3CN)CH_2^+$, respectively, can lead to protonated acrylonitrile (CH_2CHCNH^+) and propionitrile cation ($CH_3CH_2CN^+$) in the gas-phase after ion desorption. The ion peak at m/z = 60 can be assigned to the $(CH_3CN)H_3O^+$ cluster ion, what strongly agrees with the calculations of Mejías et al.,[42] in which the formation of the cluster CH_3CNH^+–H_2O occurs when H_3O^+ interacts with a single CH_3CN molecule, and the proton remains bonded to a solvating CH_3CN molecule.

Figure 4 also points to the ion desorption of the acetonitrile dimer cation $(CH_3CN)_2^+$ and the protonated acetonitrile dimer $(CH_3CN)_2H^+$ at m/z = 82 and 83, respectively. These ions are members of the $(CH_3CN)_n^+$ and $(CH_3CN)_nH^+$ ion series, whose occurrence in gas-phase experiments[51] is known. The greater desorption ion yield for the ion cluster $(CH_3CN)_2H^+$ in respect to $(CH_3CN)_2^+$ may be attributed to the production of a stronger proton-bound linear complex,[51] in which the proton is trapped symmetrically between two CH_3CN molecules, as it was predicted by Mejías et al..[42] It is remarkable that the pattern of the CH_3CN ESID spectrum observed in Figure 1 entirely repeats itself after m/z = 50. As a rule of thumb, it is possible to summarize the ESID spectrum of frozen CH_3CN by the general formula $(CH_3CN)_nX^+$, in which n = 0 – 2 and X^+ corresponds to a charged fragment generated by the dissociation of the isolated CH_3CN molecule.

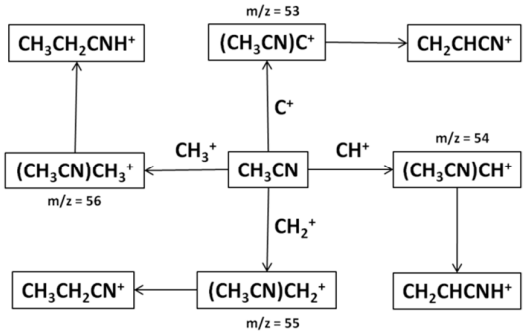

Scheme 1. Suggested reaction routes for production of acrylonitrile cation (CH_2CHCN^+), protonated acrylonitrile (CH_2CHCNH^+), propionitrile cation ($CH_3CH_2CN^+$) and protonated propionitrile ($CH_3CH_2CNH^+$) by desorption of $(CH_3CN)CH_x^+$ (x = 0–3) cluster ions.

Astrophysical implications

The ESID data presented in this study indicate a possible process by which the molecular inventory covering cold ice mantles may be incorporated into the gas-phase of molecular clouds in the ISM and, furthermore, a possible contribution to the synthesis of more complex nitrile-bearing molecules. Ion desorption under electron bombardment is initiated by Coulomb explosion of unscreened valence holes,[58] a condition matched since multiple valence holes are localized in the adsorbate for at least 10-100 fs,[36] corresponding to the ion desorption time. Multiple valence holes may be created via Auger decay of a shallow core-hole, such as the N1s, after high energy electron-impact. As shown in Figure 2, all ion desorption channels are enhanced at energies ~ 3.5 times the ionization threshold of the N1s core level. At even higher electron-impact energies, multiple excitations by the primary electron beam or excitations caused by the scattering of secondary electrons also contribute to CH_3CN fragmentation and ion desorption.

The H^+ ion is by far the most desorbed ion, since it contributes to almost 96 % of the entire ESID spectrum at 2300 eV electron bombardment. As pointed out by Pirim et al.,[59] the desorption of light fragments, such as H^+ in the present case, is a probe for determining molecular damage promoted by electron impact. The H^+ ion has the highest desorption probability and, therefore, dissociation channels on surface that may result in H^+ desorption will be best probed by ESID. By computing the ion yield for all ions desorbed from the CH_3CN ice surface, one finds the total positive ion desorption yield of $Y^+ = 5 \times 10^{-8}$ ions/electron.

Taking into account that the typical coverage of a vapour-deposited surface is on the order of ~ 10^{15} molecules cm^{-2},[60] the maximum total cross section for ion desorption from the CH_3CN ice surface is estimated to lie on the order $\sigma^+ \sim 5 \times 10^{-23}$ cm^2. Individual ion desorption cross sections σ_i^+ (in which i = fragment or cluster ion) derived in the same way are displayed in Figure 5.

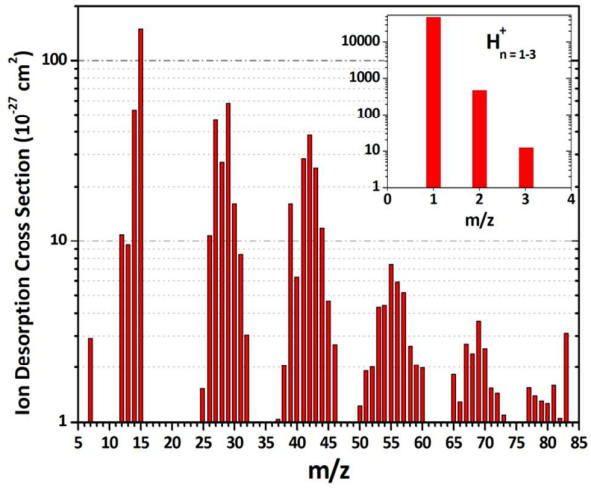

Figure 5. Cross sections derived for desorption of CH_3CN positive fragments and ion clusters due to the bombardment of 2.3 keV electrons. The inset at top right shows the ion desorption cross sections for fragments of the $H_{n=1-3}^+$ ion series.

It is noteworthy that the total cross section σ^+ derived in this work is considerably smaller than the CH_3CN desorption cross section measured by Abdulgalil and co-workers.[28] The desorption of neutral fragments, which are not observed with the present experimental setup, probably accounts for such large divergence. Cross sections for ion desorption are generally orders of magnitude smaller than those for neutral species.[60]

The desorption of protonated fragments from surfaces at cryogenic temperatures seems to be favoured by strong ion-dipole interactions and post-dissociation interactions that lead to proton-transfer reactions. Among them, CH_3CNH^+ (m/z = 42) is even more abundant than the parent molecule CH_3CN^+ (m/z = 41). As discussed by Betts and co-workers,[49] closed-shell cations are more stable due to the formation of a closed-shell species. This particular result points to the role played by ion desorption to gas-grain interactions in the ISM. The production of CH_3CNH^+ appears to be governed by a non-linear (power law) dependence on the incident electron beam current (see Figure 3). Based on the similar results of Yildirim,[54] this tendency suggests that ion collisions are necessary to induce proton-transfer reactions on the CH_3CN ice top surface.

Even though the attempts to detect CH_3CNH^+ towards the ISM have failed,[61] CH_3CNH^+ desorption to the gas of dense molecular clouds would contribute to maintain the high abundances observed for CH_3CN by dissociative electron recombination of CH_3CNH^+.[62] Through a similar pathway, complex organic molecules can be generated in the gas-phase by barrierless ion-molecule reactions or directly delivered to the gas phase after ion desorption. The latter process, would be the case for CH_2NH^+ (m/z = 29) and $CH_3NH_2^+$ (m/z = 31), whose neutral species are all known interstellar molecules.[63, 64]

It is known that gas-phase chemistry alone is unable to explain the diversity and abundance of many of the identified interstellar complex molecules.[65] Thus, grain-surface chemistry

and ion desorption are suggested to play a role in the formation of more complex gas-phase known nitriles, especially involving CH_3CN as a precursor molecule. The closely related aliphatic nitriles, propionitrile (CH_3CH_2CN), acrylonitrile (CH_2CHCN), n-butyronitrile ($CH_3(CH_2)_2CN$) and isobutyronitrile ($(CH_3)_2CHCN$), have all been detected towards the Sgr B2(N) molecular cloud.[15, 66-68] Such molecules might be formed through intra-cluster reactions involving the ion clusters $(CH_3CN)CH_{n=1-2}^+$ and $(CH_3CN)C_2H_n^+$ desorbed from the CH_3CN ice, even prior to evaporation of ice mantles covering dust grains during the warm-up phase of star-forming regions.

Regarding the Solar System, the desorbed fragments and ion clusters detected in this work are relevant to nitrile chemistry in Titan. Gas-phase CH_3CN in the upper atmosphere is expected to precipitate downward the stratosphere onto aerosol hazes, where ice clouds have been observed.[69, 70] Solar radiation, cosmic-ray bombardment and high-energy electrons trapped in the saturnian magnestophere penetrate the satellite atmosphere,[71] triggering its energetic processing. Indeed, the Ion Neutral Mass Spectrometer (INMS) probe onboard the Cassini spacecraft detected several nitrile-bearing fragments in the Titan's ionosphere, including $HCNH^+$, $CH_2NH_2^+$, CH_3CNH^+, $C_2H_3CNH^+$, $C_2H_5CNH^+$, among others.[9] It has been suggested that protonated nitriles and ion clusters might play a major role in developing proton exchange reactions that lead to the production of more complex ions and neutral molecules in the Titan's atmosphere.[72, 73] The production of protonated fragments is generally attributed to gas-phase ionizations and ion-molecule reactions, but the ESID results from this work show how some of the ions observed by the INMS probe would be delivered to the gas-phase from frozen CH_3CN molecules.

Conclusions

High energy electron impact was employed in order to simulate electron-induced processes that can occur on the surface of interstellar ice mantles covered by acetonitrile (CH_3CN) molecules and on icy condensates at the Titan's atmosphere and surface. Several fragment ions were identified by time-of-flight mass spectrometry (TOF-MS), indicating strong fragmentation of the parent molecule. Coulomb explosion following Auger electronic decay seems to be a reasonable mechanism for ion desorption, since all fragmentation channels are enhanced at energies 3.5 times the N1s ionization threshold. Predominance for protonated fragments, such as CH_3CNH^+, was observed. Such ions may be formed as the result of proton transfer reactions on surface. Collisions between dissociating products is also suggested as the first step in the production of more complex species, in the form of ion clusters. Desorption of $(CH_3CN)_2^+$ and $(CH_3CN)_2H^+$ ion clusters were readily observed, along with clusters made up of the neutral CH_3CN molecule bonded to an ion fragment of the parent molecule alone. The measured desorption ion yields were used to estimate a total desorption cross-section on the order of $\sigma^+ \sim 5 \times 10^{-23}$ cm^2, which correlates to the destruction cross-section of CH_3CN by molecular fragmentation and positive ion desorption. Our findings suggest that electron stimulated desorption from CH_3CN covered ice mantles may play a role in delivering ions to the cold interstellar and circumstellar material, which can further participate in barrierless gas-phase ion-neutral reactions. Such processes may play a role in the generation of more complex nitriles already observed in the gas-phase of star-forming regions. Similar conclusions can be ascribed to the Titan atmosphere, where a set of complex nitriles is known to exist.

Acknowledgements

The authors would like to acknowledge Conselho Nacional de Desenvolvimento Cientifico e Tecnologico (CNPq), Coordenação de Aperfeiçoamento de Pessoal de Nível Superior (CAPES), and Fundação de Amparo à Pesquisa do Estado do Rio de Janeiro (FAPERJ) for financial support.

References

1 V. Pankonin, E. Churchwell, C. Watson and J. H. Bieging, *Astrophys. J.*, 2001, **558**, 194-203.

2 P. M. Solomon, K. B. Jefferts, A. A. Penzias and R. W. Wilson, *Astrophys. J. Lett.*, 1971, **168**, L107.

3 H. E. Matthews and T. J. Sears, *Astrophys. J.*, 1983, **267**, L53-L57.

4 E. Araya, P. Hofner, S. Kurtz, L. Bronfman and S. DeDeo, *Astrophys. J. Suppl. Ser.*, 2005, **157**, 279-301.

5 V. Rosero, P. Hofner, S. Kurtz, J. Bieging and E. D. Araya, *Astrophys. J. Suppl. Ser.*, 2013, **207**, 12.

6 S. Cazaux, A. G. G. M. Tielens, C. Ceccarelli, A. Castets, V. Wakelam, E. Caux, B. Parise and D. Teyssier, *Astrophys. J.*, 2003, **593**, L51–L55.

7 V. Taquet, A. López-Sepulcre, C. Ceccarelli, R. Neri, C. Kahane and S. B. Charnley, *Astrophys. J.*, 2015, **804**, 81.

8 R. Mauersberger, C. Henkel, C. M. Walmsley, L. J. Sage and T. Wiklind, *Astron. Astrophys.*, 1991, **247**, 307-314.

9 V. Vuitton, R. V. Yelle and P. Lavvas, *Philos. Trans. R. Soc. London, A*, 2009, **367**, 729–741.

10 B. L. Ulich, *Nature*, 1974, **248**, 121-122.

11 S. D. Rodgers and S. B. Charnley, *Mon. Not. R. Astron. Soc.*, 2001, **320**, L61-L64.

12 F. Goesmann, H. Rosenbauer, J. H. Bredehöft, M. Cabane, P. Ehrenfreund, T. Gautier, C. Giri, H. Krüger, L. Le Roy, A. J. MacDermott, S. McKenna-Lawlor, U. J. Meierhenrich, G. M. M. Caro, F. Raulin, R. Roll, A. Steele, H. Steininger, R. Sternberg, C. Szopa, W. Thiemann and S. Ulamec, *Science*, 2015, **349**, aab0689.

13 K. I. Öberg, V. V. Guzmán, K. Furuya, C. Qi, Y. Aikawa, S. M. Andrews, R. Loomis and D. J. Wilner, *Nature*, 2015, **520**, 198–201.

14 E. F. van Dishoeck, *Faraday Discuss.*, 1998, **109**, 31-46.

15 A. Belloche, R. T. Garrod, H. S. P. Müller, K. M. Menten, C. Comito and P. Schilke, *Astron. Astrophys.*, 2009, **499**, 215-232.

16 E. Herbst and E. F. van Dishoeck, *Ann. Rev. Astron. Astrophys.*, 2009, **47**, 427–480.

17 C. J. Bennett, C. Pirim and T. M. Orlando, *Chem. Rev. (Washington, DC, U. S.)*, 2013, **113**, 9086-9150.
18 B. P. Mathur, L. E. Abbey, E. M. Burgess and T. F. Moran, *Org. Mass Spectrom.*, 1980, **15**, 312-316.
19 D. M. Rider, G. W. Ray, E. J. Darland and G. E. Leroi, *J. Chem. Phys.*, 1981, **74**, 1652-1660.
20 O. Neskovic, M. Veljković, D. Golobоćanin, M. Miletić and K. F. Zmbov, *Int. J. Mass Spectrom. Ion Phys.*, 1982, **44**, 61-80.
21 Y. Senba, H. Yoshida, T. Ogata, D. Sakata, A. Hiraya and K. Tanaka, *J. Electron Spectrosc. Relat. Phenom.*, 1999, **101-103**, 131–134.
22 C.-K. Huang, I.-F. Lin and S.-Y. Chiang, *Chem. Phys. Lett.*, 2007, **440**, 51–55.
23 E. Kukk, R. Sankari, M. Huttula, S. Mattila, E. Itälä, A. Sankari, H. Aksela and S. Aksela, *Int. J. Mass Spectrom.*, 2009, **279**, 69–75.
24 T. Sekitani, E. Ikenaga, K. Tanaka, K. Mase, M. Nagasono, S.-i. Tanaka and T. Urisu, *Surf. Sci.*, 1997, **390**, 107-111.
25 T. Sekitani, E. Ikenaga, H. Matsuo, S. Tanaka, K. Mase and K. Tanaka, *J. Electron Spectrosc. Relat. Phenom.*, 1998, **88-91**, 831-836.
26 E. Kukk, R. Sankari, M. Huttula, A. Sankari, H. Aksela and S. Aksela, *J. Electron Spectrosc. Relat. Phenom.*, 2007, **155**, 141–147.
27 R. L. Hudson and M. H. Moore, *Icarus*, 2004, **172**, 466–478.
28 A. G. M. Abdulgalil, D. Marchione, J. D. Thrower, M. P. Collings, M. R. S. McCoustra, F. Islam, M. E. Palumbo, E. Congiu and F. Dulieu, *Philos. Trans. R. Soc. London, A*, 2013, **371**, 20110586.
29 R. D. Ramsier and J. T. Yates Jr., *Surf. Sci. Rep.*, 1991, **12**, 243-378.
30 R. Garrod, I. H. Park, P. Caselli and E. Herbst, *Faraday Discuss.*, 2006, **133**, 51-62.
31 D. Schriver, P. Trávníčekc, M. Ashour-Abdalla, R. L. Richard, P. Hellinger, J. A. Slavin, B. J. Anderson, D. N. Baker, M. Benna, S. A. Boardsen, R. E. Gold, G. C. Ho, H. Korth, S. M. Krimigis, W. E. McClintock, J. L. McLain, T. M. Orlando, M. Sarantos, A. L. Sprague and R. D. Starr, *Planet. Space Sci.*, 2011, **59**, 2026–2036.
32 D. Drouin, A. R. Couture, R. Gauvin, P. Hovington, P. Horny and H. Demers, Monte Carlo Simulation of Electron Trajectory in Solids (CASINO), Sherbrooke: Univ. Sherbrooke, 2.42 edn., 2001.
33 F. de A. Ribeiro, G. C. Almeida, W. Wolff, H. M. Boechat-Roberty and M. L. M. Rocco, *J. Phys. Chem. C*, 2014, **118**, 25978−25986.
34 G. C. Almeida, D. P. P. Andrade, C. Arantes, A. M. Nazareth, H. M. Boechat-Roberty and M. L. M. Rocco, *J. Phys. Chem. C*, 2012, **116**, 25388−25394.
35 E. M. Williams and J. L. d. Segovia, *Vacuum*, 1989, **39**, 633-642.
36 R. Souda, *Phys. Rev. B: Condens. Matter Mater. Phys.*, 2002, **65**, 245419.
37 T. M. Orlando, A. B. Aleksandrov and J. Herring, *J. Phys. Chem. B*, 2003, **107**, 9370-9376.
38 J. Herring-Captain, G. A. Grieves, A. Alexandrov, M. T. Sieger, H. Chen and T. M. Orlando, *Phys. Rev. B: Condens. Matter Mater. Phys.*, 2005, **72**, 035431.
39 T. Tachibana, T. Miura and I. Arakawa, *Low Temp. Phys.*, 2006, **32**, 1092-1096.
40 R. N. Barnett and U. Landman, *J. Phys. Chem. A*, 1997, **101**, 164-169.
41 C. R. Cole, R. A. Outlaw, R. L. Champion, B. C. Holloway and M. A. Kelly, *Appl. Surf. Sci.*, 2007, **253**, 3789–3798.
42 J. A. Mejías, S. Hamad and S. Lago, *J. Phys. Chem. B*, 2001, **105**, 9872-9878.
43 H. Kawanowa, K. Hanatani, Y. Gotoh and R. Souda, *Surf. Rev. Lett.*, 2003, **10**, 271-275.
44 E. F. da Silveira and E. A. Schweikert, *J. Chem. Phys.*, 1988, **89**, 6708
45 J. H. D. Eland, *Rapid Commun. Mass Spectrom.*, 1996, **10**, 1560-1562.
46 S. Pilling, D. P. P. Andrade, R. Neves, A. M. Ferreira-Rodrigues, A. C. F. Santos and H. M. Boechat-Roberty, *Mon. Not. R. Astron. Soc.*, 2007, **375**, 1488–1494.
47 F. P. Netzer, J. A. D. Matthew and E. Bertel, in *Spectroscopy of Surfaces: Advances in Spectroscopy*, ed. R. J. H. Clark and R. E. Hester, John Wiley & Sons, Chichester, West Sussex, 1988, vol. 16, p. 283−376.
48 D. E. Ramaker, T. E.Madey and R. L. Kurtz, *Phys. Rev. B: Condens. Matter Mater. Phys.*, 1988, **38**, 2099-2111.
49 R. L. Betts, E. F. da Silveira and E. A. Schweikert, *Int. J. Mass Spectrom.*, 1995, **145**, 9-23.
50 F. Fantuzzi, L. Baptista, A. B. Rocha and E. F. da Silveira, *Chem. Phys.*, 2013, **410**, 109–117.
51 D. Ascenzi, P. Tosi, P. Franceschi, D. Catone, S. Turchini and K. C. Prince, *Chem. Phys.*, 2012, **398**, 269–277.
52 R. Souda, *Surf. Sci. Lett.*, 2002, **506**, L275–L281.
53 M. S. Westley, R. A. Baragiola, R. E. Johnson and G. A. Baratta, *Nature*, 1995, **373**, 405-407.
54 Y. Yildirim, M. Balcan, A. D. Bass, P. Cloutierb and L. Sanche, *Phys. Chem. Chem. Phys.*, 2010, **12**, 7950–7958.
55 S. Wagner, H. Öström, A. Kaebe, M. Krenz, M. Wolf, A. C. Luntz and C. Frischkorn, *New J. Phys.*, 2008, **10**, 125031.
56 B. Siemer, T. Hoger, M. Rutkowski, R. Treusch and H. Zacharias, *J. Phys.: Condens. Matter*, 2010, **22**, 084013.
57 B. Siemer, S. Roling, R. Frigge, T. Hoger, R. Mitzner and H. Zacharias, *Faraday Discuss.*, 2014, **168**, 553-569.
58 D. E. Ramaker, C. T. White and J. S. Murday, *Phys. Lett. A*, 1982, **89**, 211-214.
59 C. Pirim, R. D. Gann, J. L. McLain and T. M. Orlando, *Icarus*, 2015, **258**, 109–119.
60 E. M. Williams and J. L. de Segovia, *Vacuum*, 1989, **39**, 633–642.
61 B. E. Turner, T. Amano and P. A. Feldman, *Astrophys. J.*, 1990, **349**, 376-387.
62 E. Vigren, M. Kaminska, M. Hamberg, V. Zhaunerchyk, R. D. Thomas, M. Danielsson, J. Semaniak, P. U. Andersson, M. Larssona and W. D. Geppert, *Phys. Chem. Chem. Phys.*, 2008, **10**, 4014–4019.
63 P. D. Godfrey, R. D. Brown, B. J. Robinson and M. W. Sinclair, *Astrophys. Lett.*, 1973, **13**, 119-121.
64 N. Kaifu, M. Morimoto, K. Nagane, K. Akabane, T. Iguchi and K. Takagi, *Astrophys. J.*, 1974, **191**, L135-L137.
65 I. W. M. Smith, D. Talbi and E. Herbst, *Astron. Astrophys.*, 2001, **369**, 611-615.

66 Y. Miao, D. M. Mehringer, Y.-J. Kuan and L. E. Snyder, *Astrophys. J.*, 1995, **445**, L59-L62.
67 F. F. Gardner and G. Winnewisser, *Astrophys. J.*, 1975, **195**, L127-L130.
68 A. Belloche, R. T. Garrod, H. S. P. Müller and K. M. Menten, *Science*, 2014, **345**, 1584-1587.
69 R. E. Samuelson, M. D. Smith, R. K. Achterberg and J. C. Pearl, *Icarus*, 2007, **189**, 63–71.
70 R. J. de Kok, N. A. Teanby, L. Maltagliati, P. G. J. Irwin and S. Vinatier, *Nature*, 2014, **514**, 65-67.
71 M. Galand, J. Lilensten, D. Toublanc and S. Maurice, *Icarus*, 1999, **140**, 92–105.
72 G. J. Molina-Cuberos, K. Schwingenschuh, J. J. López-Moreno, R. Rodrigo, L. M. Lara and V. Anicich, *J. Geophys. Res. Planets*, 2002, **107**, 5099.
73 V. Vuitton, R.V.Yelle and M.J.McEwan, *Icarus*, 2007, **191**, 722–742.